

A mixed isogeometric plane stress and plane strain formulation with different continuities for the alleviation of locking

L. Stammen* and W. Dornisch

Chair of Structural Analysis and Dynamics
Brandenburg University of Technology Cottbus-Senftenberg
Cottbus, Germany
e-mail: {lisa.stammen,wolfgang.dornisch}@b-tu.de

Key words: Isogeometric Analysis, Mixed Formulations, Spline Basis Functions, Continuity, Locking

Abstract: *Isogeometric analysis and mixed finite element methods offer promising opportunities to enhance analysis results for complex problems like incompressible elasticity and are able to cope with different locking phenomena. In this contribution, a mixed two-field isogeometric formulation with independent approximations for displacements and stresses is derived, and its ability to counteract different types of locking is investigated using two examples. Furthermore, the influence of the continuity of the stress shape functions on the accuracy of results and convergence behaviour is shown.*

1 INTRODUCTION

Whilst finite element methods have become a common analysis method in engineering, more recent approaches involve Isogeometric Analysis (IGA), which was founded by Hughes et al. [1] and tries to unify computer aided design (CAD) and finite element analysis (FEA) by using the same model for geometry representation and analysis. Therefore, in contrast to common finite element analysis, non-uniform rational B-splines (NURBS) and other kinds of splines are used as shape functions of the finite elements instead of the usual polynomials. Due to the exact representation of the geometry, analysis results can be improved [1, 2]. Furthermore, many fast and numerically stable algorithms have been developed that exhibit favourable mathematical properties [3]. Other investigations examine the use of different kinds of splines as well [2, 4, 5]. In linear elasticity, different locking phenomena can occur while solving incompressible elasticity problems or dealing with very slender structures for instance. Mixed formulations, where stresses and/or strains or pressures are approximated independently in addition to the usual displacement approximation, can counteract these effects and lead to more accurate results [6]. Recent investigations have already combined isogeometric analysis and mixed formulations in order to benefit from the advantages of both methods [7, 8, 9, 10, 11]. Furthermore, the continuity can have a decisive influence on the accuracy of results [12]. In this contribution, a mixed isogeometric method is proposed in order to improve the analysis results and to counteract locking. Therefore, spline basis functions are used and the displacement shape functions of a two-dimensional isogeometric plane stress and plane strain element are supplemented by independent stress shape functions. These additional stress shape functions are chosen to be of one order lower compared to the displacement shape functions, but with adapted continuity. Evaluating the errors for several examples, it is shown that the proposed mixed method can lead to improved accuracy of results compared to a standard isogeometric formulation and ensures convergence even for very slender geometries and very fine and distorted meshes. Furthermore, the influence of different continuities on the convergence behavior and the accuracy of the results is investigated.

2 MIXED FINITE ELEMENT METHODS

Mixed (or hybrid) formulations approximate primary and secondary variables independently and can be derived, e.g., from weak forms [13]. The resulting finite elements can be employed to reduce locking or cope with incompressible elasticity problems [6]. A starting point for the derivation of a mixed formulation is the following three-field functional

$$\Pi_{HW}(\mathbf{u}, \boldsymbol{\epsilon}, \boldsymbol{\sigma}) = \int_{\Omega} \frac{1}{2} \boldsymbol{\epsilon}^T \mathbf{D} \boldsymbol{\epsilon} - \boldsymbol{\sigma}^T (\boldsymbol{\epsilon} - \mathbf{G} \mathbf{u}) - \mathbf{u}^T \mathbf{b} \, d\Omega - \int_{\Gamma_t} \mathbf{u}^T \bar{\mathbf{t}} \, d\Gamma - \int_{\Gamma_u} \boldsymbol{\sigma}^T (\mathbf{u} - \bar{\mathbf{u}}) \, d\Gamma, \quad (1)$$

also known as Hu-Washizu functional. In this equation, \mathbf{u} , $\boldsymbol{\epsilon}$, $\boldsymbol{\sigma}$, \mathbf{b} , $\bar{\mathbf{t}}$ and $\bar{\mathbf{u}}$ represent the displacements, strains, stresses, body forces, boundary tractions and boundary displacements, respectively. \mathbf{G} is a suitable differential operator. Using the constitutive equation

$$\boldsymbol{\epsilon} = \mathbf{D}^{-1} \boldsymbol{\sigma}, \quad (2)$$

we can derive the two-field functional

$$\Pi_{HR}(\mathbf{u}, \boldsymbol{\sigma}) = \int_{\Omega} -\frac{1}{2} \boldsymbol{\sigma}^T \mathbf{D}^{-1} \boldsymbol{\sigma} + \boldsymbol{\sigma}^T \mathbf{G} \mathbf{u} - \mathbf{u}^T \mathbf{b} \, d\Omega - \int_{\Gamma_t} \mathbf{u}^T \bar{\mathbf{t}} \, d\Gamma - \int_{\Gamma_u} \boldsymbol{\sigma}^T (\mathbf{u} - \bar{\mathbf{u}}) \, d\Gamma, \quad (3)$$

which is known as the Hellinger-Reissner functional. The variation thereof reads

$$\delta \Pi_{HR}(\mathbf{u}, \boldsymbol{\sigma}) = \int_{\Omega} -\delta \boldsymbol{\sigma}^T \mathbf{D}^{-1} \boldsymbol{\sigma} + \delta \boldsymbol{\sigma}^T \mathbf{G} \mathbf{u} + \boldsymbol{\sigma}^T \delta \mathbf{G} \mathbf{u} - \delta \mathbf{u}^T \mathbf{b} \, d\Omega - \int_{\Gamma_t} \delta \mathbf{u}^T \bar{\mathbf{t}} \, d\Gamma = 0 \quad (4)$$

for strongly fulfilled boundary conditions $\mathbf{u} = \bar{\mathbf{u}}$ on Γ_u and is known as the Hellinger-Reissner principle. In order to distinguish plane stress and plane strain formulations, the corresponding material matrix \mathbf{D} is used. For more details, see [6, 14].

3 SPLINE BASIS FUNCTIONS

3.1 Construction

Basing on a non-decreasing knot vector

$$\Xi = \{\xi_1, \dots, \xi_{n+p+1}\}, \quad \xi_i \leq \xi_{i+1}, \quad i = 1, \dots, n+p \quad (5)$$

and a predefined degree p , the construction of spline basis functions follows the following recurrence algorithm taken from [3]:

$$N_{i,0}(\xi) = \begin{cases} 1 & \text{if } \xi_i \leq \xi < \xi_{i+1} \\ 0 & \text{otherwise} \end{cases}, \quad N_{i,p}(\xi) = \frac{\xi - \xi_i}{\xi_{i+p} - \xi_i} N_{i,p-1}(\xi) + \frac{\xi_{i+p+1} - \xi}{\xi_{i+p+1} - \xi_{i+1}} N_{i+1,p-1}(\xi) \quad (6)$$

The corresponding derivatives of the B-spline basis function are calculated by

$$N'_{i,p} = \frac{p}{\xi_{i+p} - \xi_i} N_{i,p-1}(\xi) - \frac{p}{\xi_{i+p+1} - \xi_{i+1}} N_{i+1,p-1}(\xi) \quad (7)$$

A NURBS surface \mathbf{S} can then be represented by

$$\mathbf{S}(\xi, \eta) = \sum_{i=1}^n \sum_{j=1}^m R_{i,j}(\xi, \eta) \mathbf{P}_{i,j} \quad (8)$$

where $R_{i,j}$ are the piece-wise rational basis functions defined by

$$R_{i,j}(\xi, \eta) = \frac{N_{i,p}(\xi) N_{j,q}(\eta) \omega_{i,j}}{\sum_{k=1}^n \sum_{l=1}^m N_{k,p}(\xi) N_{l,q}(\eta) \omega_{k,l}} \quad (9)$$

In these formulas, $\mathbf{P}_{i,j}$ denotes the control points building up the control net of the surface and $\omega_{i,j}$ represents their corresponding weights. In the following chapters the number of local basis functions will be referred to by $n_{en} = (p+1)(q+1)$ and the total number of global basis functions is denoted by $n_{np} = n \cdot m$.

3.2 Refinement and continuity

There are two refinement methods for B-Splines, which are recalled according to [2]: The first refinement method increases the number of basis functions by inserting additional knots (*knot insertion*). Thereby, the insertion of one knot leads to an increase in the number of basis functions by 1. As this is equal to dividing an element, this method is often called *h-refinement* in comparison to standard finite element methods. The second refinement method elevates the polynomial order by 1 (*order elevation*). As both methods are hierarchical refinement methods, each of the original basis function can be expressed as linear combination of the refined basis functions.

Based on these two refinement methods, two combined refinement procedures can be derived for isogeometric analysis. If knot insertion is performed before order elevation, this is called *p-refinement*. In this way, one basis function is added for each element. Using *k-refinement*, the spline order is elevated first and subsequently knot insertion is performed. In contrast to *p-refinement*, this method inserts less basis functions. Furthermore, maximal continuity is obtained, while *p-refinement* yields meshes with limited continuity. Figure 1 depicts the influence of the continuity on the shape functions for $p = 3$:

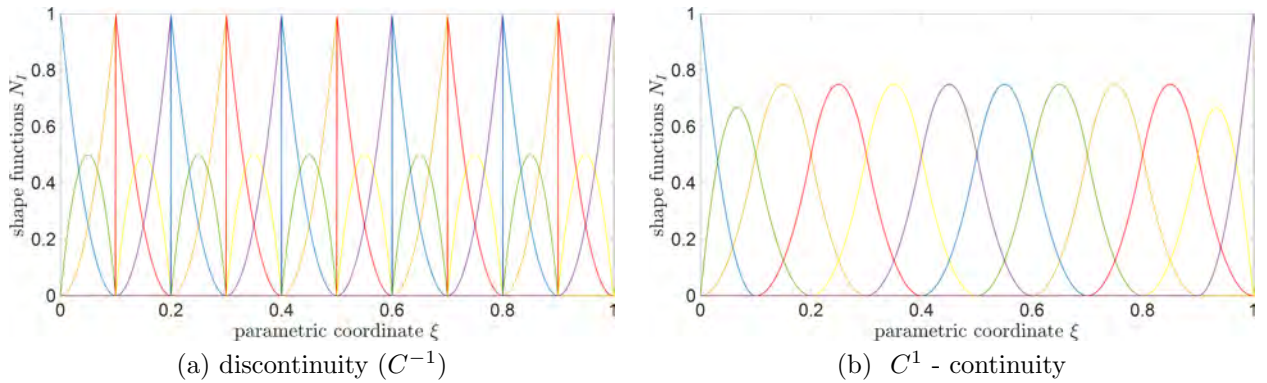


Figure 1: Influence of the continuity on the shape functions for $p = 3$

4 MIXED ISOGEOMETRIC ELEMENTS WITH TWO UNKNOWN FIELDS

Depending on which unknown fields are chosen, different mixed isogeometric finite elements can be developed from the corresponding variational principle. In this publication the \mathbf{u} - $\boldsymbol{\sigma}$ -mixed formulation, that was derived in [15] for instance, shall be used and adapted to isogeometric analysis.

The chosen fields are approximated by independent shape functions as follows:

$$\mathbf{u}^h = \sum_{I=1}^{n_{en}^u} N_I^u \mathbf{u}_I \quad \text{and} \quad \boldsymbol{\sigma}^h = \sum_{I=1}^{n_{en}^\sigma} N_I^\sigma \boldsymbol{\sigma}_I \quad (10)$$

with

$$\mathbf{u}_I = \begin{pmatrix} u_{I1} \\ u_{I2} \end{pmatrix} \quad \text{and} \quad \boldsymbol{\sigma}_I = \begin{pmatrix} \sigma_{I1} \\ \sigma_{I2} \\ \tau_{I12} \end{pmatrix}. \quad (11)$$

Thus, the strain-displacement relation becomes:

$$\boldsymbol{\epsilon}^h = \begin{pmatrix} \epsilon_{11}^h \\ \epsilon_{22}^h \\ 2\gamma_{12}^h \end{pmatrix} = \mathbf{G} \mathbf{u}^h = \sum_{I=1}^{n_{en}^u} \mathbf{B}_I^u \mathbf{u}_I, \quad (12)$$

where

$$\mathbf{B}_I^u = \begin{bmatrix} N_{I,1}^u & 0 \\ 0 & N_{I,2}^u \\ N_{I,2}^u & N_{I,1}^u \end{bmatrix} \quad (13)$$

contains the partial derivatives of the displacement shape functions in the first and second direction ($N_{I,1}^u$ and $N_{I,2}^u$). The interpolation of the variations of \mathbf{u} , $\boldsymbol{\epsilon}$ and $\boldsymbol{\sigma}$ read

$$\delta \mathbf{u}^h = \sum_{I=1}^{n_{en}^u} N_I^u \delta \mathbf{u}_I, \quad \delta \boldsymbol{\epsilon}^h = \sum_{I=1}^{n_{en}^u} \mathbf{B}_I^u \delta \mathbf{u}_I \quad \text{and} \quad \delta \boldsymbol{\sigma}^h = \sum_{I=1}^{n_{en}^\sigma} N_I^\sigma \delta \boldsymbol{\sigma}_I. \quad (14)$$

Inserting these relations into equation (4) leads to

$$\begin{aligned} \delta \Pi_{HR}^h(\mathbf{u}^h, \boldsymbol{\sigma}^h) &= \sum_{I=1}^{n_{en}^\sigma} \sum_{J=1}^{n_{en}^u} \delta \boldsymbol{\sigma}_I^T \int_{\Omega} N_I^\sigma \mathbf{B}_J^u \, d\Omega \, \mathbf{u}_J \\ &+ \sum_{I=1}^{n_{en}^u} \sum_{J=1}^{n_{en}^\sigma} \delta \mathbf{u}_I^T \int_{\Omega} \mathbf{B}_I^{uT} N_J^\sigma \, d\Omega \, \boldsymbol{\sigma}_J \\ &- \sum_{I=1}^{n_{en}^\sigma} \sum_{J=1}^{n_{en}^\sigma} \delta \boldsymbol{\sigma}_I^T \int_{\Omega} N_I^\sigma \mathbf{D}^{-1} N_J^\sigma \, d\Omega \, \boldsymbol{\sigma}_J \\ &- \sum_{I=1}^{n_{en}^u} \delta \mathbf{u}_I^T \left[\int_{\Omega} N_I^u \mathbf{b} \, d\Omega + \int_{\Gamma_t} N_I^u \bar{\mathbf{t}} \, d\Gamma \right] = 0. \end{aligned} \quad (15)$$

The control point displacements \mathbf{u}_I can now be assembled in the vector

$$\hat{\mathbf{u}} = \left(\mathbf{u}_1^T, \mathbf{u}_2^T, \dots, \mathbf{u}_{n_{np}^u}^T \right)^T, \quad (16)$$

where n_{np}^u denotes the number of control points in the displacement mesh. The control point stresses are assembled analogously in

$$\hat{\boldsymbol{\sigma}} = \left(\boldsymbol{\sigma}_1^T, \boldsymbol{\sigma}_2^T, \dots, \boldsymbol{\sigma}_{n_{np}^\sigma}^T \right)^T, \quad (17)$$

where n_{np}^σ denotes the number of control points in the stress mesh. The virtual displacements and virtual stresses $\delta \hat{\mathbf{u}}$ and $\delta \hat{\boldsymbol{\sigma}}$ are interpolated akin. Replacing the summations in equation (15) by matrix multiplications leads to:

$$\delta \Pi_{HR}^h(\mathbf{u}^h, \boldsymbol{\sigma}^h) = \delta \hat{\boldsymbol{\sigma}}^T \hat{\mathbf{C}} \hat{\mathbf{u}} + \delta \hat{\mathbf{u}}^T \hat{\mathbf{C}}^T \hat{\boldsymbol{\sigma}} + \delta \hat{\boldsymbol{\sigma}}^T \hat{\mathbf{A}} \hat{\boldsymbol{\sigma}} - \delta \hat{\mathbf{u}}^T \hat{\mathbf{f}}^u = 0 \quad (18)$$

This equation needs to be fulfilled for every arbitrary test function $\delta \hat{\boldsymbol{\sigma}}$ and $\delta \hat{\mathbf{u}}$ and can hence be splitted in two parts, which can be written in standard matrix form. This leads to the following global system of equations

$$\begin{bmatrix} \hat{\mathbf{A}} & \hat{\mathbf{C}} \\ \hat{\mathbf{C}}^T & \mathbf{0} \end{bmatrix} \begin{pmatrix} \hat{\boldsymbol{\sigma}} \\ \hat{\mathbf{u}} \end{pmatrix} = \begin{pmatrix} \mathbf{0} \\ \hat{\mathbf{f}}^u \end{pmatrix}. \quad (19)$$

In a standard manner, these matrices are calculated at the element level and later assembled to the global system. Thus, using the n_{en}^u and n_{en}^σ shape functions which have influence in the respective element e , equation (15) results in:

$$\delta \Pi_{HR}(\mathbf{u}^h, \boldsymbol{\sigma}^h) = \bigcup_{e=1}^{n_{el}} \left[\delta \hat{\boldsymbol{\sigma}}^{eT} \hat{\mathbf{C}}^e \hat{\mathbf{u}}^e + \delta \hat{\mathbf{u}}^{eT} \hat{\mathbf{C}}^{eT} \hat{\boldsymbol{\sigma}}^e + \delta \hat{\boldsymbol{\sigma}}^{eT} \hat{\mathbf{A}}^e \hat{\boldsymbol{\sigma}}^e - \delta \hat{\mathbf{u}}^{eT} \hat{\mathbf{f}}^{ue} \right] = 0 \quad (20)$$

Defining

$$\hat{\mathbf{v}}^e = \begin{pmatrix} \hat{\boldsymbol{\sigma}}^e \\ \hat{\mathbf{u}}^e \end{pmatrix} \quad \text{and} \quad \delta \hat{\mathbf{v}}^e = \begin{pmatrix} \delta \hat{\boldsymbol{\sigma}}^e \\ \delta \hat{\mathbf{u}}^e \end{pmatrix} \quad (21)$$

results in the more comprehensive form

$$\delta \Pi_{HR}(\mathbf{u}^h, \boldsymbol{\sigma}^h) = \bigcup_{e=1}^{nel} \left[\delta \hat{\mathbf{v}}^{eT} \hat{\mathbf{K}}^e \hat{\mathbf{v}}^e - \delta \hat{\mathbf{v}}^{eT} \hat{\mathbf{f}}^e \right] = 0 \quad , \quad (22)$$

where

$$\hat{\mathbf{K}}^e = \begin{bmatrix} \hat{\mathbf{A}}^e & \hat{\mathbf{C}}^e \\ \hat{\mathbf{C}}^{eT} & \mathbf{0} \end{bmatrix} \quad (23)$$

is the system matrix at element level and

$$\hat{\mathbf{f}}^e = \begin{pmatrix} \mathbf{0} \\ \hat{\mathbf{f}}^{ue} \end{pmatrix} \quad (24)$$

is the element load vector. The submatrices are computed by:

$$\begin{aligned} \hat{\mathbf{A}}^e &= - \int_{\Omega^e} \mathbf{N}^{\sigma T} \mathbf{D}^{-1} \mathbf{N}^{\sigma} \, d\Omega \\ \hat{\mathbf{C}}^e &= \int_{\Omega^e} \mathbf{N}^{\sigma T} \mathbf{B}^u \, d\Omega \\ \hat{\mathbf{f}}^{ue} &= \int_{\Omega^e} \mathbf{N}^{uT} \mathbf{b} \, d\Omega + \int_{\Gamma_t^e} \mathbf{N}^{uT} \bar{\mathbf{t}} \, d\Gamma \quad . \end{aligned} \quad (25)$$

The displacement shape functions N_I^u , which are assembled in

$$\mathbf{N}^u = [N_1^u \mathbf{1} \quad N_2^u \mathbf{1} \quad \cdots \quad N_{n_{en}^u}^u \mathbf{1}] \quad , \quad (26)$$

are determined as described in chapter 3.1. The stress shape functions N_I^σ are assembled analogously in \mathbf{N}^σ , where $\mathbf{1}$ is the identity matrix of the dimension 2 and 3, respectively. In standard finite element formulations, the number of necessary additional stress variables has to fulfill the stability condition

$$n_\sigma \geq n_u \quad (27)$$

for a two field approach, where $\boldsymbol{\sigma}$ is the primary variable and \mathbf{u} is the constraint variable [6]. In this formula n denotes the number of degrees of freedom of the respective variable. Whether this condition is sufficient in Isogeometric Analysis as well has to be investigated in further studies. The additionally introduced stress variables can be condensed out, resulting in the final equation

$$\hat{\mathbf{C}}^T \hat{\mathbf{A}}^{-1} \hat{\mathbf{C}} \hat{\mathbf{u}} = -\hat{\mathbf{f}}^u \quad . \quad (28)$$

In the next section, the procedure leading to the shape functions for the two chosen fields is described.

5 DETERMINATION OF THE REQUIRED BASIS FUNCTIONS

For the presented mixed isogeometric method, displacements and stresses are chosen as two unknown fields and approximated independently. Thereby, the stress shape functions are chosen to be of one order lower than the displacement shape functions. Furthermore, the continuity of the stress shape functions can be adapted to study the effect on the analysis results. This is implemented in *MATLAB* [16] by using different refinement procedures on the original surface geometry, yielding two different meshes used for the displacements and the stresses, respectively. This procedure is depicted in Figure 2. The resulting meshes are exemplified in Figure 3. The corresponding shape functions can be seen in Figure 4.

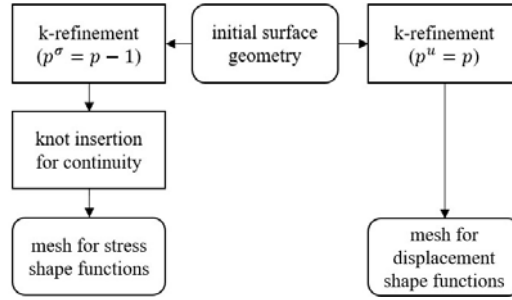


Figure 2: Refinement procedure for the generation of the two different meshes for the displacement and the stress shape functions using k-refinement for different degrees

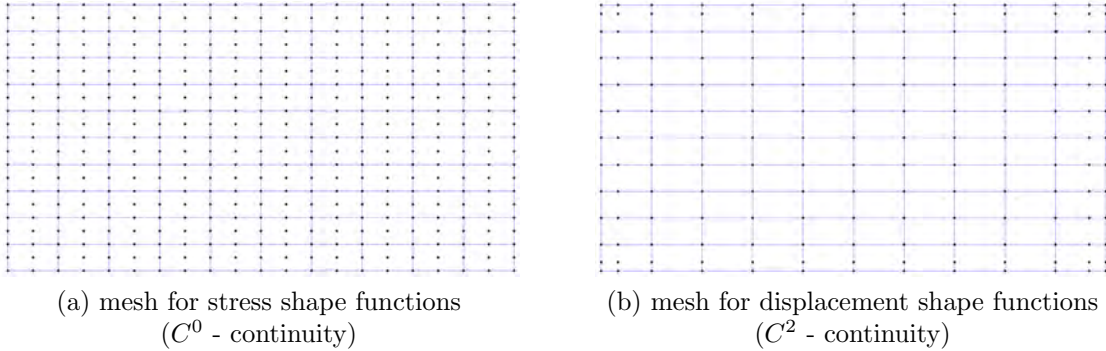


Figure 3: Resulting meshes for a rectangular domain divided into 10 elements per direction with their respective control points using $p^u = 3$ and $p^\sigma = 2$

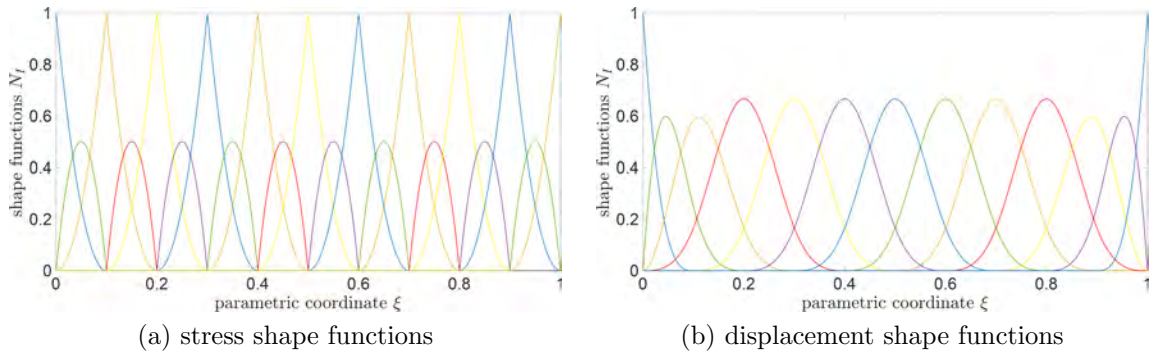


Figure 4: Resulting shape functions for the meshes depicted in Figure 3

6 NUMERICAL EXAMPLES

In this section, the ability of the proposed mixed formulation to counteract different types of locking and the influence of the continuity of the stress shape functions is investigated. Therefore, the results of the proposed mixed isogeometric formulation are compared to the results of a standard (pure displacement based) isogeometric formulation. Within these investigations, for the mixed approach, the continuity of the stress shape functions is varied, whereas the continuity of the displacement shape functions is set to maximal continuity C^{p^u-1} using k-refinement, according to the procedure depicted in Figure 2. The continuity of the shape functions for the standard formulation is varied between C^0 and maximal continuity C^{p-1} by using p- and k-refinement, respectively. Starting with the initial geometry, all meshes are refined regularly and equally in both directions using quadrilateral elements.

6.1 Beam subjected to pure bending

Firstly, a beam under pure bending is investigated. The initial distorted geometry including its control points (red) and relevant material and loading data is indicated in Figure 5.

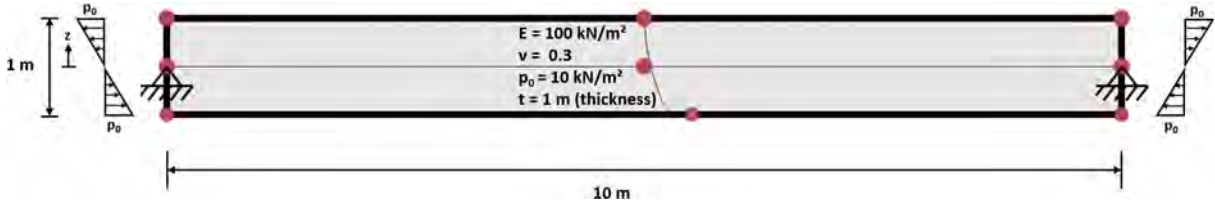
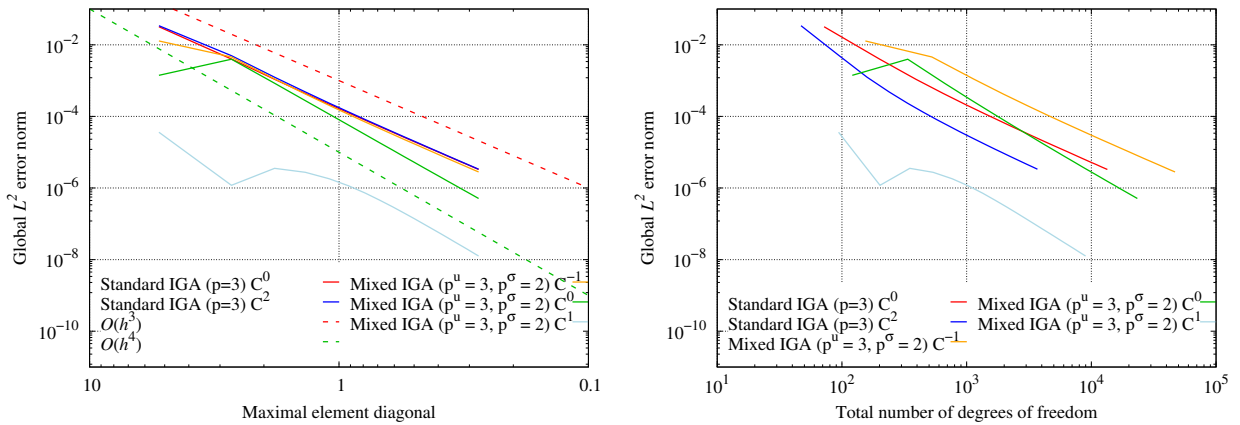


Figure 5: Initial geometry, material and loading data of beam subjected to pure bending

In order to investigate the ability of the formulation to counteract in-plane shear locking, a linearly varying load is applied on both vertical edges for the depicted distorted mesh and the results of the proposed mixed formulation are compared to the analytical solution given in equation (29) using the L^2 -error norm of the stresses as indicated in equation (30).

$$\sigma_x(z) = 2 \cdot p_0 \cdot \frac{z}{h}, \quad \sigma_z = 0 \text{ kN/m}, \quad \tau_{xz} = 0 \text{ kN/m} \quad (29)$$

$$\|\Delta\sigma\|^2 = \sqrt{(\sigma_x - \sigma_x^h)^2 + (\sigma_y - \sigma_y^h)^2 + (\tau_{xy} - \tau_{xy}^h)^2} \quad (30)$$



(a) dependent on the maximal element diagonal (b) dependent on the number of degrees of freedom

Figure 6: Comparison of the L^2 error norm of stresses for the beam subjected to pure bending

As can be seen in Figure 6(a), the proposed mixed isogeometric formulation yields better results compared to a standard isogeometric formulation, for which only a minor difference between C^0 - and C^2 - continuity can be recognized for this example. Whereas no significant benefit can be achieved by the mixed formulation using discontinuous (C^{-1}) stress shape functions, the use of C^0 - continuity offers a better convergence rate ($O(h^4)$) than the standard formulation ($O(h^3)$). Particularly interesting is the behavior for C^1 - continuous stress shape functions, since proper convergence behavior begins later as in the other graphs, while constantly offering a much better result. This only holds if the L^2 - error norm is calculated using the results of the introduced stress parameters (eq.(17)). If the stresses used for the calculation of the L^2 -error norm are directly recalculated from the displacement parameters (eq.(16)), no benefit of the introduced mixed formulation can be observed compared to the standard formulation, and even partly worse results are achieved for C^1 - continuity of the stress shape functions of

the mixed formulation. In order to maintain the benefits resulting from the introduced stress parameters if static condensation is used for the proposed mixed formulation, the stresses need to be recalculated using the equation

$$\hat{\sigma} = -\hat{A}^{-1} \hat{C} \hat{u} \quad . \quad (31)$$

Taking into account the number of degrees of freedom (cf. 6(b)), the benefits of the mixed formulation only hold for C^1 - continuous stress shape functions. Lower continuities offer worse results for the same number of degrees of freedom compared to the standard formulation, for which the benefit of C^2 - continuity is the lower number of degrees of freedom.

Figure 6 depicts the results for a slenderness ratio of 10. Varying the slenderness of the beam as the critical parameter (by reducing its height), the results of the mixed formulation are constantly better as those of the standard formulation. If the height is reduced to 0.001 m (increasing the slenderness ratio to 10000), the standard formulation diverges, whereas the proposed mixed formulation ensures convergence even for very slender structures.

6.2 Cook's Membrane

The Cook's Membrane is a standard problem to examine the robustness of finite element formulations. The initial geometry and a sample mesh are depicted in Figure 7.

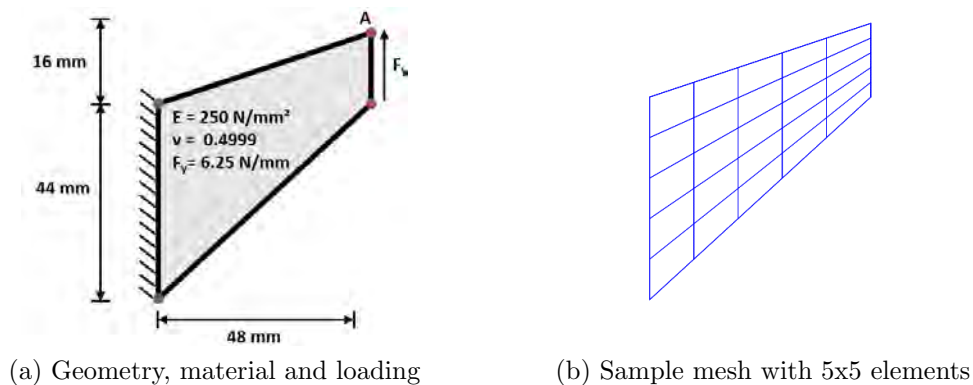


Figure 7: Data of Cook's Membrane problem

The relevant material and loading parameters were chosen to enable the comparison to the results presented in [17] and in order to investigate the ability of the presented formulation to cope with an incompressible elasticity problem and the resulting locking effects. Therefore, the vertical displacement of point A is compared to the reference solution (black lines in Figure 8 and Figure 9) taken from [17]. As can be observed in Figure 8, the mixed formulation offers better results in comparison to the standard formulation with maximal continuity. Using C^0 -continuous shape functions, much better results can be obtained by the standard formulation for this example. Compared to this, the mixed formulation is only beneficial using stress shape functions with maximal continuity $C^{p^\sigma-1}$. However, in this case, the results oscillate between even and odd numbers of elements per direction. Hence, the stability of the mixed method obviously depends on the continuity of the stress shape functions. Examining the eigenvalues of the system matrix for this example, spurious zero eigenvalues occurred for maximal continuity of the stress shape functions, which may cause this instability. This issue will be investigated in detail in further studies. Considering only the results for even numbers of elements (dashed lines), the convergence behavior is superior compared to all graphs. The lower the degree of the shape functions is, the more locking occurs. Thus, the mixed formulation offers a higher benefit for the lowest possible degree of shape functions (cf. Figure 8 (a), (b)). Taking into account the

number of degrees of freedom resulting from the chosen continuity (cf. Figure 9), the benefit of the mixed formulation for maximal continuity of the stress shape functions becomes obvious (considering only even numbers of elements per direction). Especially for higher degrees, the use of C^0 -continuous shape functions for the standard formulation loses its benefit in this context.

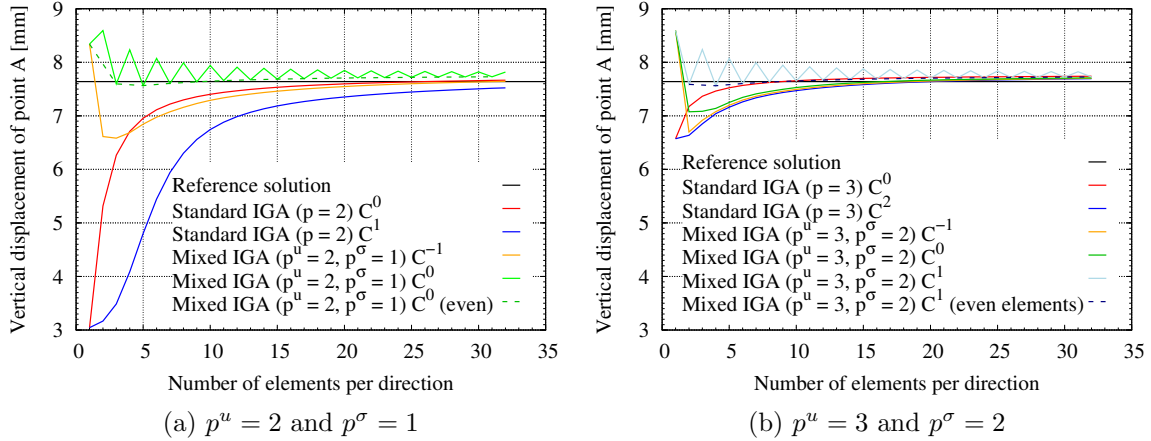


Figure 8: Comparison of the resulting vertical displacement of point A in dependence of the number of elements per direction

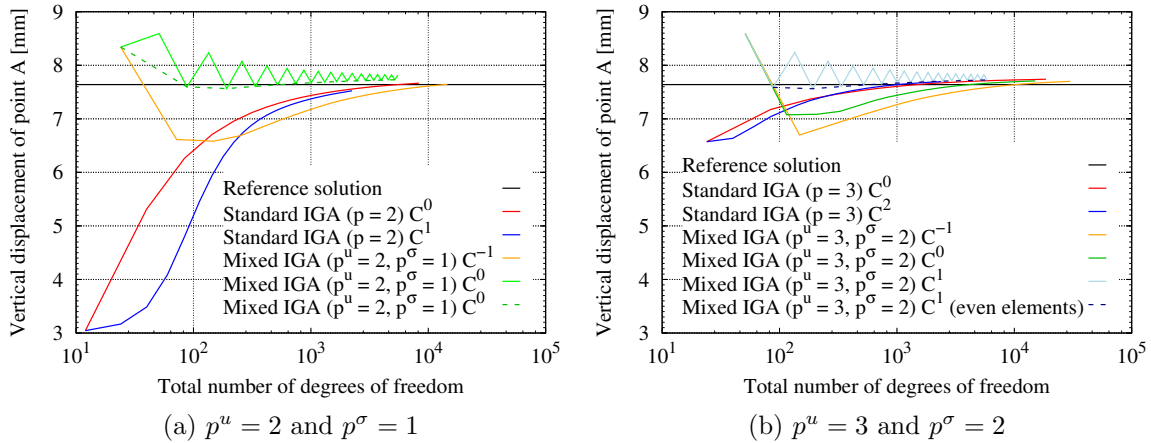


Figure 9: Comparison of the resulting vertical displacement of point A in dependence of the total number of degrees of freedom

7 CONCLUSIONS

In this contribution, a mixed isogeometric method is derived and its ability to counteract different locking effects is studied for a plane stress and a plane strain example. Furthermore, the influence of the continuity of the stress shape functions is investigated. It is shown that a mixed isogeometric formulation can yield results with a higher convergence rate compared to a standard formulation and is able to counteract different locking phenomena. Additionally, increasing the continuity of the stress shape functions yields better results of the proposed mixed formulation but can yield instabilities due to spurious zero eigenvalues for maximal continuity, despite offering the best results. Further research will focus on the stability for maximal continuity of the stress shape functions. Furthermore, different ansatz spaces for the stress shape functions should be investigated.

REFERENCES

- [1] Cottrell, J.A., Hughes, T.J.R. and Bazilevs, Y. *Isogeometric Analysis: Towards integration of CAD and FEA*. John Wiley & Sons, 2009.
- [2] de Borst, R., Crisfield, M.A., Remmers, J.J.C. and Verhoosel, C.V. *Nonlinear Finite Element Analysis of Solids and Structures*. John Wiley & Sons, 2012.
- [3] Piegl, L. and Tiller, W. *The NURBS Book*. Springer, 1997.
- [4] Hllig, K. *Finite Element Methods with B-Splines*. Society for Industrial and Applied Mathematics, 2003.
- [5] Mner, B. *B-Splines als Finite Elemente*. Shaker, 2006.
- [6] Zienkiewicz, O.C., Taylor, R.L. and Zhu, J.Z. *The finite element method: Its basis and fundamentals*. 6th Edition, Elsevier Butterworth-Heinemann, 2005.
- [7] Echter, R., Oesterle, B. and Bischoff, M. A hierarchic family of isogeometric shell finite elements. *Comput. Methods Appl. Mech. Eng.*, Vol. **254**, pp. 170-180, (2013).
- [8] Bouclier, R., Elguedj, T. and Combescure, A. Efficient isogeometric NURBS-based solid-shell elements: Mixed formulation and \bar{B} -method. *Comput. Methods Appl. Mech. Eng.*, Vol. **265**, pp. 86-110, (2013).
- [9] Bouclier, R., Elguedj, T. and Combescure, A. An isogeometric locking-free NURBS-based solid-shell element for geometrically nonlinear analysis. *Int. J. Numer. Methods Eng.*, Vol. **101**, pp. 774-808, (2015).
- [10] Bieber, S., Oesterle, B., Ramm, E. and Bischoff, M. A variational method to avoid locking - independent of the discretization scheme. *Int. J. Numer. Methods Eng.*, Vol. **114**, pp. 801-827, (2018).
- [11] Zou, Z., Scott, M.A., Miao, D., Bischoff, M., Oesterle, B. and Dornisch, W. An isogeometric ReissnerMindlin shell element based on Bzier dual basis functions: Overcoming locking and improved coarse mesh accuracy. *Comput. Methods Appl. Mech. Eng.*, Vol. **370**, 113283, (2020).
- [12] Adam, C., Bouabdallah, S., Zarroug, M and Maitournam, H. Improved numerical integration for locking treatment in isogeometric structural elements, Part I: Beams. *Comput. Methods Appl. Mech. Eng.*, Vol. **279**, pp. 1-28, (2014).
- [13] Reddy, J.N. *An Introduction to the Finite Element Method*. McGraw-Hill, 2006.
- [14] Knothe, K. and Wessels, H. *Finite Elemente: Eine Einfhrung fr Ingenieure*. Springer Berlin Heidelberg, 2008.
- [15] Pian, T.H.H. and Sumihara, K. Rational approach for assumed stress finite elements. *Int. J. Num. Meth. Eng.*, Vol. **20**, pp. 1685-1695, (1984).
- [16] The MathWorks, Inc. *MATLAB* (Version R2019b). Natick, Massachusetts, 2019.
- [17] Bombarde, D.S., Nandy, A. and Gautam, S.S. A Two-Field Formulation in Isogeometric Analysis to Alleviate Locking. *Advances in Engineering Design: Select Proceedings of FLAME 2020.*, pp. 191-199, (2021).